Special Collection

Electroreductive 5-Hydroxymethylfurfural Dimerization on Carbon Electrodes

Ricarda Kloth,*[a, b] Dmitry V. Vasilyev,[a] Karl J. J. Mayrhofer,[a, b] and Ioannis Katsounaros*[a]

The electrochemical conversion of biomass-based compounds to fuels and fuel precursors can aid the defossilization of the transportation sector. Herein, the electrohydrodimerization of 5-hydroxymethylfurfural (HMF) to the fuel precursor 5,5′-bis (hydroxymethyl)hydrofuroin (BHH) was investigated on different carbon electrodes. Compared to boron-doped diamond (BDD) electrodes, on glassy carbon (GC) electrodes a less negative HMF reduction onset potential and a switch in product selectivity from BHH to the electrocatalytic hydrogenation product 2,5-di(hydroxymethyl)furan (DHMF) with increasing overpotential was found. On BDD, the electrohydrodimerization was the dominant process independent of the applied potential. An increase in the initial HMF concentration led to suppression of the competing hydrogen evolution reaction and DHMF formation, resulting in higher BHH faradaic efficiencies. In contrast, BHH selectivity decreased with higher initial HMF concentration, which was attributed to increased electrochemically induced HMF degradation. Finally, it was demonstrated that even a simple graphite foil can function as an active HMF electroreduction catalyst.

Introduction

The extensive fossil fuel consumption, excessive CO_2 emission, and the concomitant anthropogenic climate change demand technological developments that enable the valorization of renewable resources. Fuel technologies that are in line with a closed carbon cycle economy are particularly attractive to prevent further contributions to global warming. Thus, biofuels based on non-edible biomass are considered as an important pillar on the route towards defossilization of the transportation sector.[1] 5-Hydroxymethylfurfural (HMF), a platform chemical derived from lignocellulose, has gained increasing research interest in the last decade[2] as it shows great potential for further valorization into fuels[3] and other value-added chemicals.[4] Many studies to generate biofuels from HMF have centered around its hydrogenolysis to 2,5-dimethylfuran (DMF).[5] Additionally, strategies for C–C bond formation have been devised, such as aldol condensation[6] or dimerization reactions,[7] to elongate the carbon chain length for obtaining C_8–C_{15} compounds in the diesel or jet fuel range. However, classical organic chemistry dimerization concepts such as the pinacol coupling were found to be unsuitable for the HMF valorization due to the tendency for HMF degradation and polymerization under the applied conditions.[8]

A promising alternative to the conventional organic chemistry approach is the electrochemical dimerization of HMF to the pinacol coupling product as it comprises several advantages.[9] Firstly, it avoids the usage of expensive and potentially toxic reducing agents, since electrons are directly donated to the reactant by the electrode, which results in higher atom efficiency, lower cost, and reduced waste generation. Additionally, high pressure and temperature as well as the use of organic solvents can be avoided, as electrochemistry is usually performed at room temperature in aqueous solutions. Secondly, by utilizing renewable solar, wind, or geothermal electricity, the biofuel production becomes a completely sustainable process based only on biomass and green electrical energy. Furthermore, the process will allow the profitable usage of the electrical energy excess generated by the fluctuating renewable power supply. Finally, electrosynthesis offers the advantage of driving two valorization reactions with the same power input, so that an oxidation and a reduction reaction can be performed simultaneously. This concept of paired electrolysis has already been demonstrated for the HMF conversion, resulting in the formation of 2,5-di(hydroxymethyl)furan (DHMF) on the cathode and 2,5-furandicarboxylic acid (FDCA) on the anode side of the electrolyzer.[10]

So far, literature on reductive electrochemical HMF conversion focused primary on DHMF and other products generated through electrocatalytic hydrogenation (ECH),[10,11] while electrohydrodimerization was mentioned only as an undesired side reaction[10,11d–f] (Scheme 1). The product of the HMF electrohydrodimerization, 5,5′-bis(hydroxymethyl)hydrofuroin (BHH), has been isolated, identified, and quantified only by Li and co-workers,[10] while Benito and co-workers[11e,f] hypothesized the

[a] R. Kloth, Dr. D. V. Vasilyev, Prof. Dr. K. J. J. Mayrhofer, Dr. I. Katsounaros
Forschungszentrum Jülich GmbH
Helmholtz Institute Erlangen-Nürnberg for Renewable Energy (IEK-11)
Egerlandstr. 3, 91058 Erlangen (Germany)
E-mail: r.kloth@fz-juelich.de
i.katsounaros@fz-juelich.de
[b] R. Kloth, Prof. Dr. K. J. J. Mayrhofer
Department of Chemical and Biological Engineering
Friedrich-Alexander University Erlangen-Nürnberg
Egerlandstr. 3, 91058 Erlangen (Germany)

Supporting information for this article is available on the WWW under https://doi.org/10.1002/cssc.202101575

This publication is part of a collection of invited contributions focusing on "The Fuel Science Center – Adaptive Conversion Systems for Renewable Energy and Carbon Sources". Please visit to view all contributions.

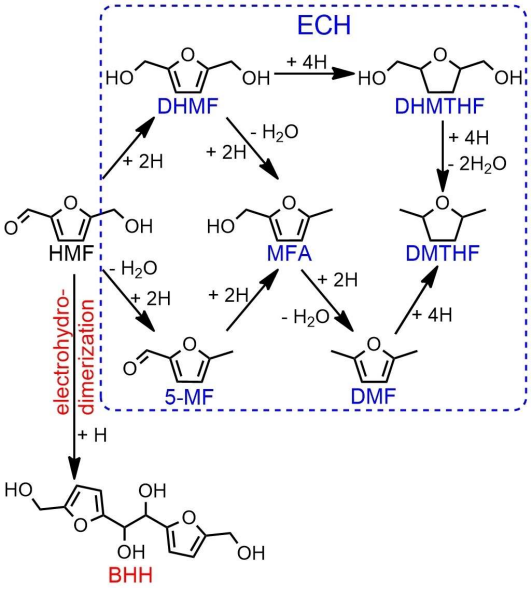

Scheme 1. Electrochemical HMF reduction pathways grouped in ECH reactions yielding DHMF, 5-methylfurfuryl alcohol (MFA), 5-methylfurfural (5-MF), DMF, 2,5-dimethyltetrahydrofuran (DMTHF), and 2,5-bis (hydroxymethyl)-tetrahydrofuran (DHMTHF), and electrohydrodimerization yielding BHH. The descriptor "H" symbolizes the transfer of electrons and protons necessary for the formation of the respective products without indicating the details on the mechanism of these reactions.

structure based on mass spectrometry and chromatography analyses.

In contrast, in this work we focus on BHH as the target compound because this electrochemically accessible and biomass-based C_{12} product has ideal perquisites as a diesel or jet fuel precursor. According to literature on furfural electrohydrodimerization,[12] electrodes that require high overpotential to enable the hydrogen evolution reaction (HER), such as Pb or carbon materials, are favorable dimerization catalysts, whereas ECH reactions are dominant on catalysts that are active for the HER. In addition, when carbon is used as support for nanoparticle catalysts, HMF dimerization is promoted as found by Chadderdon et al.[10a] Therefore, we focus on carbon materials as electrocatalysts for this study as they offer additional advantages in comparison to metal catalysts.[13] First, carbon is a highly abundant material in contrast to many precious metal catalysts, and it is non-toxic, unlike other metal catalysts with high HER overpotential, such as Pb or Hg. Furthermore, carbon electrodes are in agreement with the principles of green chemistry[14] since they can be additionally derived from biomass, which in combination with the advantages of electrochemistry improves the general greenness of the reaction process. For this work, glassy carbon (GC) and boron-doped diamond (BDD) were chosen as representatives of sp^2- and sp^3-hybridized carbon materials, respectively, to investigate into the effect of the hybridization of the electrode on the HMF reduction activity and selectivity. Furthermore, the effects of applied electrode potential and initial HMF concentration are discussed. We find a less negative HMF reduction onset potential on the sp^2 carbon electrode in comparison to the sp^3 material and a switch in product selectivity from the electrohydrodimerization product BHH to the ECH product DHMF with increasing overpotential. On BDD, on the other hand, the dimer BHH is the major quantifiable product independent of the applied potential. On GC, an increase in the initial HMF concentration leads to a suppression of ECH product formation and of the HER, as well as to an increase in the BHH faradaic efficiency. However, it also decreases the selectivity towards BHH, which we attribute to enhanced electrochemically induced HMF degradation processes. Finally, we demonstrate that even cheap, simple graphite foil can function as an active HMF electrohydrodimerization catalyst for the facile production of BHH as a green biofuel precursor.

Results and Discussion

Comparison of sp^2 and sp^3 carbon materials

First, the effect of the hybridization of the carbon electrode on the HMF reduction reaction was investigated. GC was chosen as a representative of the sp^2-hybridized materials because it offers a well-defined and stable surface for electrochemical measurements,[15] while a BDD electrode represented the sp^3-hybridized carbon. For the following discussion, we assume that the hybridization is the major factor that causes the observed differences between BDD and GC.[16] However, possible contributions of boron as an active site in BDD cannot be excluded;[17] a detailed evaluation of this effect is out of the scope of this work. In a first step, cyclic voltammetry (CV) was performed to assess the activity of the two materials towards the HMF reduction reaction (Figure 1).

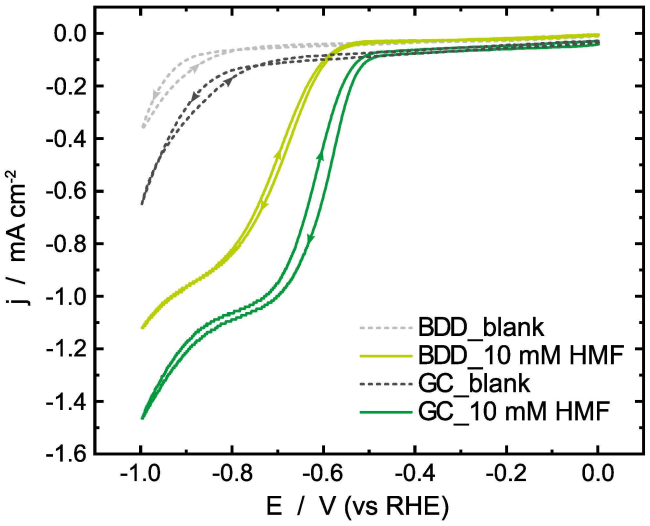

Figure 1. Cyclic voltammograms of BDD and GC in 0.1 M carbonate buffer (blank) and with addition of 10 mM HMF performed in a scanning flow cell setup at a scan rate of 5 $mV\,s^{-1}$. Both materials are active HMF electroreduction catalysts with GC showing a less negative onset potential than BDD.

In the blank voltammograms, obtained in pure carbonate buffer, only the HER occurs at large overpotentials, and the known higher activity of GC for this reaction in comparison with BDD is confirmed.[16,18] In the presence of HMF, both carbon electrodes demonstrate an earlier onset of the reductive current than the respective blanks, which clearly indicates the additional HMF electroreduction. The rate of HMF reduction becomes limited by mass transport at high overpotentials before the HER sets in (similar to other carbon materials such as carbon black[10a]). The overlap of the mass-transport-limited HMF reduction and the superimposed HER manifests as a shoulder in the recorded current in this potential range. The onset potential for the HMF reduction on GC is approximately −0.5 V, while on BDD the reaction onset potential is slightly more negative by about 50 mV.

To obtain quantitative information on the product distribution of the reactions on the two catalysts, steady-state electrolysis in the potential region from −0.6 to −1.0 V vs. reversible hydrogen electrode (RHE) was performed, and the formed products were quantified with high-performance liquid chromatography (HPLC) and gas chromatography. Special care was taken during the construction of the electrolysis setup that the majority of known HMF reduction products (Scheme 1) and H_2, as the side product from water splitting, could be identified and quantified. For example, the gaseous outlet stream from the electrolyzer passes through a series of cold traps before entering the gas chromatograph, in order to capture DMF that evaporates from the electrolyte due to continuous degassing.[19] Additionally, HMF was purified by vacuum sublimation (see Section S1 in the Supporting Information) to prevent any side reactions with possible impurities and ensure that all observed products stem from the electrolysis procedure.

Figure 2 shows the effect of applied potential on the selectivity, faradaic efficiency, and formation rates of the three major reaction products (DHMF, BHH, and H_2) observed on BDD and GC. Besides the three mentioned products, other known HMF-derived compounds are only formed in negligible amounts under the applied conditions (<1% selectivity and faradaic efficiency for each of the compounds). However, a considerable amount of still unidentified compounds is produced on these carbon materials, as indicated by the loss in the mass and charge balance for the HMF reduction reaction on both electrodes (see fraction of unknowns in Figure 2). Based on preliminary data, we believe that this fraction of unknown compounds is a mixture that majorly consists of HMF degradation products in addition to a variety of products formed through further dimerization reactions. The HMF degradation during the electrolysis is indicated by a change in color of the electrolyte solution from colorless to yellowish, which points towards the polymerization of HMF to humins.[20] The formation of additional dimerization products besides BHH during electrolysis is indicated by several points. First, the HPLC chromatograms of samples taken after the electroreduction (Figure S2a, b) show a series of peaks with retention times between 9 and 11.5 min that could not be assigned to known reaction products. These reaction products can be assumed to be structurally very similar due to the overlapping of multiple peaks in the chromatogram and additionally less polar than HMF, DHMF, or BHH since they elute at later retention times due to stronger interactions with the nonpolar stationary phase. Analysis of these peaks with liquid chromatography mass spectrometry (LC-MS) using a direct analysis in real time (DART) ion source[21] revealed that these compounds exhibit masses in the range of HMF dimerization products. However, due to the

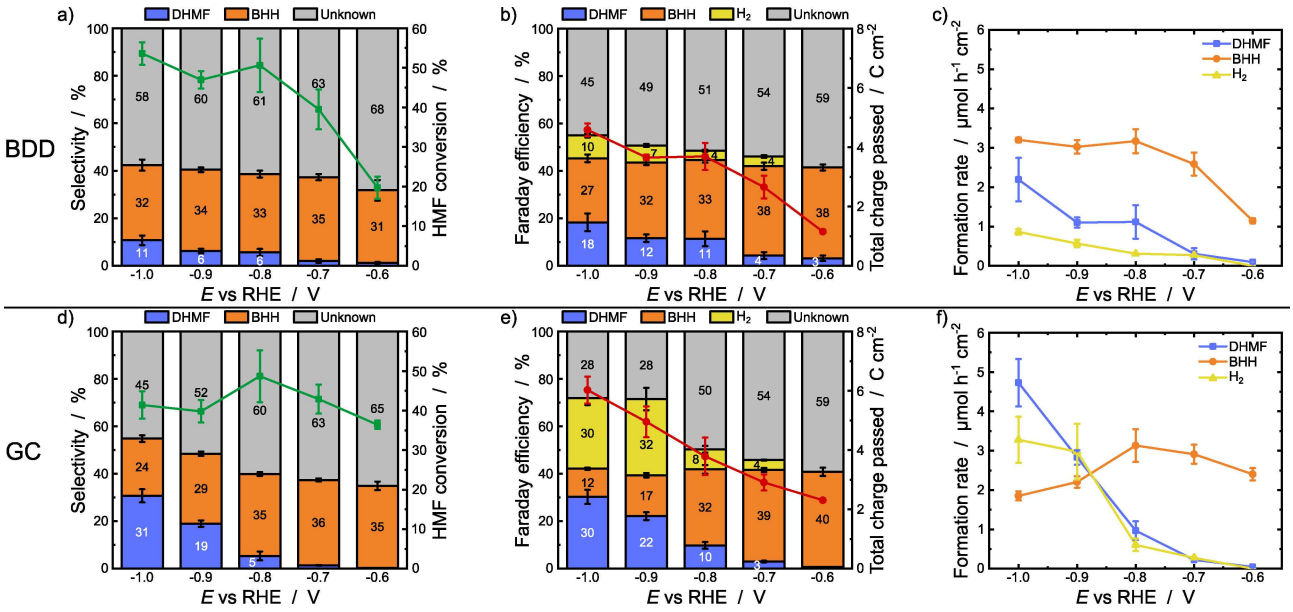

Figure 2. Steady-state electrolysis of HMF at various potentials on BDD and GC. (a) Selectivity (columns) and HMF conversion (lines), (b) faradaic efficiency (columns) and total charge passed (lines), and (c) average formation rates of the three major reaction products DHMF, BHH, and H_2 on BDD. (d–f) Corresponding data obtained on GC. Electrolysis conditions: 10 mM HMF in 0.1 M carbonate buffer (pH 9.2), 2 h reaction time. All values are averaged from at least three measurements.

poor separation of the peaks on the HPLC column and the complex mass spectra created by the DART ion source, specific information on the exact molecular masses of the compounds could not be obtained. Finally, we performed ^{1}H NMR spectroscopy of these unknowns, and the obtained spectra are giving a hint towards HMF dimerization products (Figure S4). A complete structural characterization of these was, however, sophisticated, as the submitted samples contained mixtures of compounds at minor concentrations, which made peak assignment difficult. To analyze if the unknown products might be derivatives of the dimer BHH, we performed electrolysis using BHH as the starting material and found that BHH was electrochemically inactive under the conditions applied here. Therefore, these not yet identified dimerization products are most likely produced in a parallel route to BHH. Further work needs to be devoted to identifying these compounds in order to better understand the reaction mechanism and fully explore the potential of this reaction. Throughout this work, we assume that the percentage of unidentified compounds consist of a mixture of multiple minor products, so that DHMF and BHH formation are the major electrocatalytic reactions occurring under the conditions applied here. This claim is supported by the low peak heights of the unidentified compounds in the HPLC chromatogram (Figure S2), which shows that none of these products is formed in high quantities. Furthermore, ^{1}H NMR spectroscopy of the electrochemically created product mixture implies that no products are formed in high amounts besides DHMF and BHH (Figure S5).

Contemplating Figure 2, a trend of simultaneously increasing DHMF and H_2 selectivity, faradaic efficiency, and formation rate with decreasing potential can be observed on both electrodes. This is in agreement with the proposed mechanisms of surface-adsorbed hydrogen (H*) being involved in DHMF formation through ECH[10a] and in the HER through the Volmer step.[22] While the Volmer step accelerates with decreasing potentials, the H* coverage increases, leading to enhanced DHMF and H_2 formation. In contrast, both electrodes show high selectivity, faradaic efficiency, and formation rates for the dimer BHH already at low overpotentials, where DHMF and H_2 formation are still minimal or even not occurring. This observation supports that the dimerization reaction of HMF does not involve H* and rather proceeds by an outer-sphere mechanism, as proposed by Chadderdon et al. for the similar electrohydrodimerization reaction of furfural to hydrofuroin.[12a] A comparison of the here observed potential dependencies of the selectivity and faradaic efficiency of DHMF, H_2, and BHH with the data obtained by Chadderdon et al. on carbon black electrodes[10a] shows that our findings are in good agreement with the trends reported by them.

The comparison of GC and BDD reveals that on the sp^3 carbon electrode the dimerization reaction is favored over DHMF formation and HER independent of the applied potential, as demonstrated by the higher selectivities, faradaic efficiencies, and formation rates for BHH compared to the other products (Figure 2a–c). On GC, on the other hand, BHH is the major product only at low overpotentials (formation of $\approx$2.8 μmol h^{-1} cm^{-2} in average), while at more negative potentials (−0.9 and −1.0 V) the BHH formation rate decreases and gets surpassed by the formation rates of DHMF and H_2. This trend is also reflected in the product selectivities and faradaic efficiencies. These differences between the two electrodes can be explained by considering the higher HER activity of GC than BDD[16,18] and by contemplating the role of protons in the reaction mechanisms towards the two competing HMF reduction products BHH and DHMF. Due to sp^2 carbons being more active towards the HER than sp^3 BDD, the H* surface coverage is higher on GC than on BDD at the same potentials. Hence, the ECH of HMF to DHMF and the HER become more favorable on the GC electrode than the HMF dimerization. Since DHMF and BHH are the products of competing HMF reaction pathways (Scheme 1), the suppression of the dimerization reaction on GC at potentials more negative than −0.8 V can be explained by the depletion of HMF (from the fast ECH reaction) and protons (from the HER and the ECH reactions). As the overall HMF conversion is rather unaffected by the applied potential on GC within our electrolysis setup ($\approx$42% in average, see Figure 2d), a strong increase in DHMF formation goes at the expense of the formation of other products. On BDD, on the other hand, the ECH and HER activity is lower, so that electrohydrodimerization is always the favored reaction route and a plateau in the BHH formation rate of around 3.1 μmol h^{-1} cm^{-2} is observed. The comparably low BHH formation rate on BDD at the most positive potential of −0.6 V is the result of the more negative HMF reduction onset potential on BDD. In this case, the overall HMF conversion after electrolysis is only 20%, which correlates to the currents observed during the CV experiment (Figure 1).

Considering all observed properties of BDD and GC for the electrochemical HMF reduction process, it can be concluded that both materials are active HMF reduction catalysts with specific advantages and disadvantages, which render them suitable for different applications. BDD, for example, would be suitable for applications where no precise potential control is possible, since the target product BHH is always formed with highest selectivity and faradaic efficiency of all known products and undesired ECH side reactions and the HER are minimal. However, BDD also shows a lower activity for the HMF reduction reaction at low overpotentials in comparison to GC, which is an unfavorable property for cost-efficient electrolysis. GC, on the other hand, exhibits high BHH formation rates, faradaic efficiencies, and selectivities already at low overpotentials where DHMF formation and HER are still slow. In addition to the typically lower costs for sp^2 carbon materials in comparison to the rather expensive sp^3 BDD or some metal catalysts, these properties render sp^2 carbons a very interesting and promising class of catalyst materials for the HMF electrohydrodimerization. It is, however, important to maintain a stable, appropriate potential during the electrolysis on this material to control the reaction selectivity.

Effect of the initial HMF concentration

In a next step, the influence of the initial HMF concentration on the product distribution was studied in order to optimize the

reaction conditions and increase the yield of the dimerization target product (Figure 3). Based on the general mechanism of a dimerization reaction, an increase in the yield of the dimer product is expected when the concentration of the starting material is increased, as has already been observed for the electrochemical HMF reduction on polycrystalline Ag.[10a] For this study, GC was chosen as the working electrode due to its high activity at low overpotentials as discussed above. All experiments were carried out at a constant potential of −0.8 V, since the previous experiments showed the highest BHH formation rate at this potential, while the ECH and HER side reaction rates were still relatively low.

The HMF conversion in our system is rather constant at approximately 46% after 2 h of electrolysis independent of the initial HMF concentration (Figure 3a), which suggests that the dominating reactions follow a first-order reaction kinetic behavior. This is supported by the linear dependence of the BHH formation rate on the initial HMF concentration, displayed in Figure S6. Additionally, it is another indicator towards the mechanism of BHH formation being an outer-sphere reaction, as an inner-sphere mechanism would result in a fractional reaction order between 0 and 1 due to limited availability of adsorption sites at high HMF concentrations. Furthermore, a decrease in selectivity and faradaic efficiency for the DHMF formation as well as suppression of the HER is observed when the initial HMF concentration is increased. For BHH, on the other hand, an increase in the faradaic efficiency is observed with increasing initial HMF concentration, which is in agreement with the general dimerization mechanism. We attribute the observed suppression of DHMF and H_2 formation at high initial HMF concentrations to the competition for protons with the fast outer-sphere dimerization reaction. At high initial HMF concentrations, the increased BHH formation rate can lead to a depletion of protons near the electrode surface, so that the formation of H* and the corresponding HER and DHMF formation are suppressed. In contrast to the faradaic efficiency, the selectivity for BHH is decreasing simultaneously with the initial HMF concentration. A plausible explanation for these opposing trends can be non-electrochemical reactions, which are more pronounced in more concentrated solutions and contribute to the conversion of HMF that is used in the calculation of BHH selectivity.

Such pathway for non-electrochemical HMF consumption can be the homogeneous HMF degradation to humins, which is favored in alkaline environment[20a] and in concentrated HMF solutions.[20b] Based on control experiments, we exclude that severe homogeneous HMF degradation takes place in the bulk solution under our conditions (pH 9.2) for all HMF concentrations tested. However, the degradation reaction can be accelerated at the interface, which likely becomes more alkaline during electrolysis than the bulk solution, due to proton consumption from the reduction reactions, despite the use of a buffer electrolyte.[23] Another possible HMF consumption route would be electrochemically induced chain reactions, which consume several molecules of HMF per exchanged electron and thus have little impact on the faradaic efficiency for HMF reduction products. To validate these hypotheses, however, further product analysis of formed humins and thorough mechanistic investigations are required.

In conclusion, it can be noted that the best relation of BHH to ECH and HER product formation rates was achieved at the highest HMF concentration tested here (Figure S6). However, an increase in initial HMF concentration also leads to higher non-electrochemical but electrochemically induced HMF consumption to untargeted side products, which reduces the overall selectivity of the reaction towards BHH. In order to balance these two effects, an intermediate concentration must be chosen for efficient HMF conversion.

Graphite as cheap carbon material electrode

Based on the promising HMF reduction characteristics found for BDD and GC, we investigated if simple graphite could also function as an active and selective catalyst for the HMF electrohydrodimerization. The performance of the graphite foil was compared to the HMF electroreduction behavior of GC to investigate the differences between these two sp^2 carbon types.

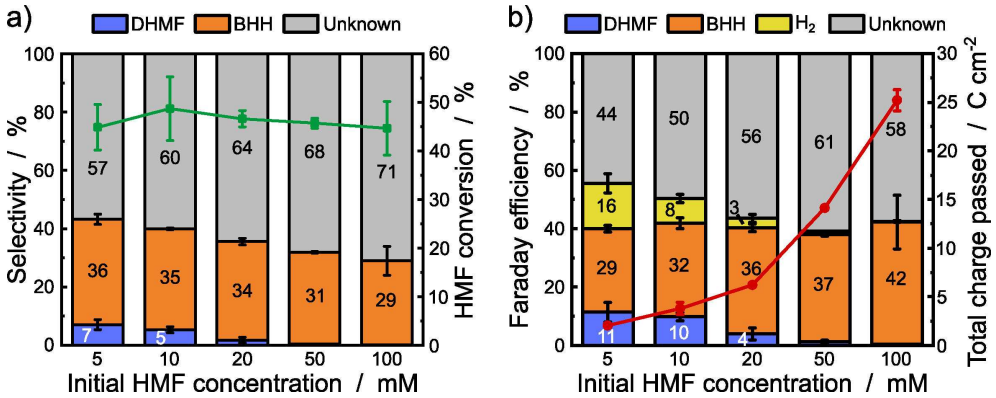

Figure 3. Effect of the initial HMF concentration on the HMF electroreduction. (a) HMF conversion (line) and product selectivity (columns) and (b) total charge passed (line) and faradaic efficiency (columns) of the three major products BHH, DHMF, and H_2. Electrolysis conditions: 0.1 M carbonate buffer supporting electrolyte (pH 9.2), $E = -0.8$ V, 2 h reaction time. All values are averaged from at least three measurements.

Similar to GC, graphite exhibits an onset potential of approximately −0.5 V for this reaction and a shoulder in the cyclic voltammogram when the HER sets in (Figure 4). The differences between the two materials in non-faradaic current are most likely resulting from a higher surface area of the graphite foil in comparison to the mirror-like GC. The inset of Figure 4 displays the formation rates of the three major products obtained during steady-state electrolysis at −0.7 V on GC and graphite, respectively. While the DHMF and H_2 formation rates are higher on graphite than on GC, the formation rate of BHH is decreased slightly to 2.6 μmol h^{-1} cm^{-2}. Similar trends are observed when comparing product faradaic efficiencies and selectivities of these two materials (Figure S7). This suggests that the H* formation is more facile on graphite than on GC, which is probably related to different surface structures and active sites.

These experiments demonstrate that even simple and cheap carbon materials are able to perform as HMF electroreduction catalysts. This encourages further research on the electrocatalytic activity of the broad family of carbon materials for the HMF electrohydrodimerization to investigate in greater detail the effects of, for example, different carbon surface structures, preparation procedures, and heteroatoms.

Conclusion and Outlook

Herein, we investigated the performance of different carbon materials as catalysts for the electrohydrodimerization of 5-hydroxymethylfurfural (HMF) to the fuel precursor 5,5′-bis (hydroxymethyl)hydrofuroin (BHH). Additionally, the effects of applied potential and initial HMF concentration on the product distribution were examined to guide the optimization of reaction conditions for high target product yields. A lower overpotential for the HMF electroreduction was found on sp^2 glassy carbon (GC) in comparison to the sp^3 boron-doped diamond (BDD) electrode. Furthermore, independent of the applied potential, on BDD the dimer BHH was found to be the major quantifiable product, while GC exhibited a switch in product selectivity from BHH to 2,5-di(hydroxymethyl)furan (DHMF) and a strong increase in hydrogen evolution reaction (HER) at more negative potentials. This suggests different preferential applications of these two materials. An increase in the initial HMF concentration led to suppression of HER and the electrocatalytic hydrogenation (ECH) product DHMF, while an increase in BHH faradaic efficiency was observed. However, higher HMF concentrations also resulted in reduced selectivity of the process, probably due to increased non-electrochemical HMF consumption caused by electrochemically induced side reactions. We propose a tentative scheme for the HMF reduction reaction that includes all known reaction pathways (Scheme 2). Thereby, we want to create awareness for the so far unidentified reaction pathways and point out that further work is necessary to clarify the mechanism of these side reactions and the exact nature of the products to be able to purposefully optimize the reaction parameters. Finally, a simple graphite foil was successfully applied as HMF electroreduction catalyst and found to be comparable in activity to GC. Further research on other carbon materials such as carbon paper, carbon fibers, or nanostructured carbon should be conducted to fully explore the potential of these materials for efficient HMF electroreduction.

In order to close the mass and charge balance and gain deeper understanding of the reaction mechanism, we deem it important to identify the still unknown products observed in

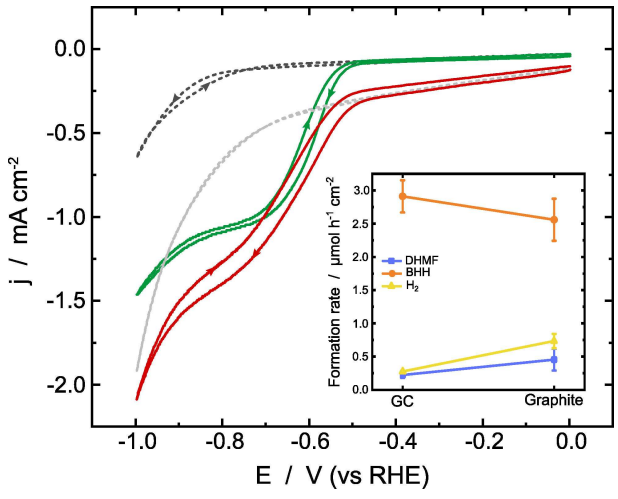

Figure 4. Cyclic voltammograms obtained on GC (dark grey) and graphite (light grey) in 0.1 M carbonate buffer and with addition of 10 mM HMF (GC: green, graphite: red) performed in a scanning flow cell setup at a scan rate of 5 mV s^{-1}. The inset shows the formation rates for the three main products DHMF, BHH, and H_2 observed during a 2 h electrolysis at −0.7 V in 10 mM HMF in 0.1 M carbonate buffer (pH 9.2) in the steady-state electrolysis setup. The values are averaged from at least three measurements.

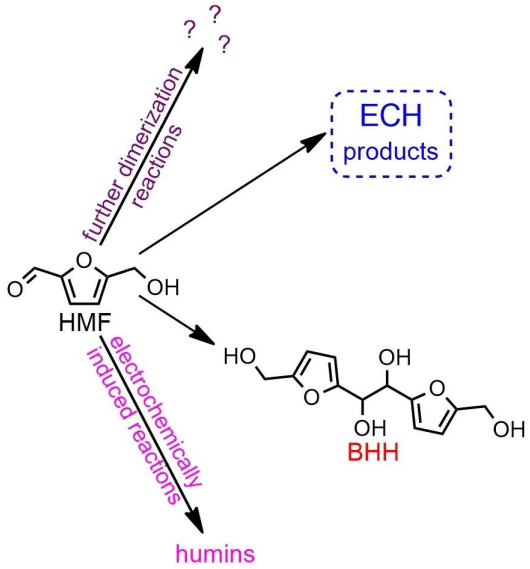

Scheme 2. Electrochemical HMF reduction reaction scheme displaying the additional pathways for electrochemically induced HMF consumption and the formation of unidentified dimerization products in a parallel reaction to the BHH formation.

the HPLC chromatogram (Figure S2). Based on preliminary data, we assume that these unidentified compounds are most likely HMF dimerization products, which are formed in parallel to the dimer BHH (Scheme 2). These compounds would also be of value as fuels or fuel precursors due to their C_{12} backbone, so that the overall yield of HMF electrohydrodimerization products of the reaction would increase and the atom efficiency and overall greenness of the reaction would improve. However, better separation of the unknown compounds in the HPLC chromatogram is necessary for successful product identification and quantification, so that future work should be devoted to the optimization of the analytics. Additionally, efficient dimer product extraction and hydrogenation techniques need to be developed to obtain a feasible production process for renewable, green fuels based on biomass-derived HMF. Finally, we believe that this work will help researchers working with carbon-supported electrocatalysts to assess the role of their support in the HMF conversion reaction and distinguish it from the investigated catalyst.

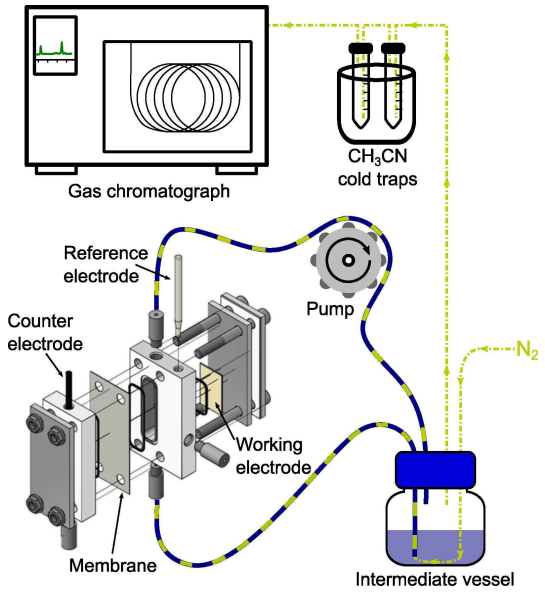

Scheme 3. Steady-state electrolysis setup based on a three-electrode two-compartment electrolyzer in a flow configuration. The acetonitrile-filled cold traps were used to capture the evaporated DMF, while H_2 quantification was performed with an online gas chromatograph.

Experimental Section

Materials and chemicals

Sodium bicarbonate, sodium carbonate, and DMF were obtained from Alfa Aesar. HMF, 5-MF, DMTHF, DHMTHF, sulfuric acid, benzyl alcohol, acetonitrile (HPLC gradient grade), and acetonitrile-d3 ($\geq$ 99.8 at.% D) were purchased from Sigma Aldrich. DHMF was obtained from Cayman Chemical and MFA from Acros Organics. All solutions were prepared using ultrapure (18 MΩ cm) water from a Milli-Q IQ 7000 system (Merck). GC plates were obtained from HTW Germany. BDD electrodes were purchased from Condias and details on the material characteristics can be found in the work by Hutton et al.[24] Graphite foil was purchased from Alfa Aesar and Ir mixed metal oxide (MMO) plates as counter electrodes were obtained from Metakem.

Scanning flow cell setup

An electrochemical scanning flow cell (SFC) was used to measure CV curves for all carbon materials. The principles and details of SFC are provided in previous publications.[25] In brief, the SFC consists of a v-shaped flow channel with a circular opening at the bottom under which the working electrode is positioned. In our case, the SFC was equipped with an Ag/AgCl (3 M KCl, BASi) reference electrode and a Pt wire (Goodfellow) counter electrode. The circular opening exposed a geometric working electrode area of 0.125 cm^2 to the electrolyte, and an electrolyte flow rate of 1 mL min^{-1} through the cell was realized using a Reglo ICC peristaltic pump (Ismatec).

Steady-state electrolysis setup

The steady-state electrolysis setup (Scheme 3) was based on an in-house built two-compartment electrochemical cell, as described in detail in a previous publication.[26] As working electrodes, different carbon materials were applied with 4 cm^2 of surface area exposed to the electrolyte, while an Ir MMO plate served as the counter electrode in all cases. The working and counter electrode compartments were separated by a bipolar membrane (Fumasep BPM) and an Ag/AgCl electrode (3 M KCl, BASi) was used as the reference. The electrolyzer cell was operated in a flow configuration with 30 mL electrolyte volume cycling continuously through the working electrode compartment and an intermediate vessel using a Reglo ICC peristaltic pump (Ismatec) at around 20 mL min^{-1}. N_2 at a flow rate of 5 mL min^{-1} (controlled by a mass flow controller from Bronkhorst) was used to remove oxygen from the electrolyte and withdraw gaseous products from the reactor. Therefore, the tube for N_2 purging was inserted into the catholyte inlet tubing within the intermediate vessel, so that N_2 gas bubbles and electrolyte were traversing the reactor simultaneously. By this means, electrochemically generated gaseous species were continuously flushed into the intermediate vessel, which resulted in the formation of a homogeneous gas phase for reproducible product analysis. However, the purging of the electrolyte with inert gas led to DMF evaporation from the system due to its low water miscibility and high volatility.[5a] To recapture the DMF, the outlet gas stream from the purge vessel was directed through two cold traps filled with 10 mL CH_3CN each and cooled in an ice bath. Thereby, 80% of the DMF could be recaptured in the cold traps, while 2% remained in the electrolyte and around 18% were still evaporated, as determined with control experiments. After passing through the cold traps, the gas stream was subjected to an online gas chromatograph, which performed sample injections approx. every 8.5 min throughout the electrolysis for H_2 quantification.

Electrochemical measurements

All electrochemical measurements, either in the SFC or the steady-state electrolysis setup were performed with a Reference 600 potentiostat (Gamry) using 0.1 M carbonate buffer with pH 9.2 as the supporting electrolyte and purified HMF (see the Supporting Information) at varying concentrations. We chose the carbonate buffer system for our work instead of the so far more typical borate buffer due to its lower toxicity while still providing buffering capacity in the desired pH range. The ohmic resistance of the setup was determined prior to every experiment by electrochemical impedance spectroscopy (EIS) and compensated for 85% by

applying positive feedback.[27] Throughout this work, the potentials are displayed in the RHE scale and current densities are calculated based on the geometric electrode area exposed to the electrolyte. The conversion from the Ag/AgCl reference electrode to RHE was performed with the following Equation (1):

$$E_{RHE} = E_{(Ag/AgCl)} + 0.21\,V + 0.059 \times pH \quad (1)$$

CV was performed in the SFC setup in the potential region from 0.0 to −1.0 V vs. RHE at a scan rate of 5 $mV\,s^{-1}$. For the steady-state electrolysis experiments, chronoamperometry measurements at different potentials were performed for 2 h. Each electrolysis was reproduced at least three times. The carbon working electrodes were treated by the following procedures prior to use: GC was manually polished with diamond paste. The BDD electrode underwent an anodic pretreatment at 10 $mA\,cm^{-2}$ for 10 min in 0.1 M sulfuric acid. The graphite foil was used as received and a fresh piece was employed for every experiment.

Product analysis

All HMF-derived compounds were analyzed with an Infinity II 1260 HPLC (Agilent Technologies) equipped with a diode array UV detector. The separation was performed using an InfinityLab Poroshell 120 EC-C18 column (3×150 mm, particle size 2.7 μm; Agilent Technologies) at 25 °C, an injection volume of 10 μL, and gradient elution with water and acetonitrile. The elution procedure started with an increase in the acetonitrile fraction from initially 3 to 25 vol% within the first 15 min at a constant flow rate of 0.5 $mL\,min^{-1}$. In the 15–20 min time period, the acetonitrile fraction was increased to 50 vol% and the flow rate increased to 0.7 $mL\,min^{-1}$ followed by a final isocratic hold at these conditions for 3.5 min. Compound identification and quantification were performed using commercially available standards, except for the two BHH isomers where fraction collection and NMR spectroscopy were utilized to obtain the standards (see the Supporting Information for more details). Table S1 summarizes the retention times and UV absorption maxima of all tested possible HMF electroreduction products.

Gaseous H_2 was quantified using a Clarus 590 (PerkinElmer) gas chromatograph in a modified model 1117 version (ARNL6513). This instrument is equipped with a thermal conductivity detector (TCD) and a flame ionization detector (FID) and able to separate gas mixtures containing H_2, He, O_2, N_2, CO, CO_2, H_2S, CH_4, C_2H_6, C_2H_4, and C_2H_2 using a series of columns and an elaborate valve switching sequence. In this configuration, H_2 is separated on a HayeSep T and a Molecular Sieve 5A column at a constant temperature of 60 °C and detected with the TCD. A calibration curve for quantifying H_2 was generated by performing chronopotentiometry experiments at different current densities in pure buffer solution. By assuming 100% faradaic efficiency for the HER in the buffer solution and taking into account the N_2 carrier gas flow rate, the recorded peak areas could be correlated to the H_2 formation rate [$mol\,s^{-1}$] resulting in a linear calibration curve (Figure S3). The calibration measurements were performed within our electrolysis setup, in order to calibrate at the same conditions as used in our electrochemical measurements.

Based on the product quantification, the HMF conversion as well as product selectivities, faradaic efficiencies and formation rates were calculated (see the Supporting Information for equations).

Acknowledgements

This research has been funded by the Deutsche Forschungsgemeinschaft (DFG, German Research Foundation) under Germany's Excellence Strategy – Exzellenzcluster 2186 "The Fuel Science Center" – ID: 390919832. D.V.V. acknowledges funding from the Alexander von Humboldt Foundation (reference 3.3-RUS-1215116-HFST–P). Open Access funding enabled and organized by Projekt DEAL.

Conflict of Interest

The authors declare no conflict of interest.

Keywords: 5-hydroxymethylfurfural · biomass upgrading · dimerization · electrocatalysis · renewable fuels

[1] A. D. Korberg, B. V. Mathiesen, L. R. Clausen, I. R. Skov, *Smart Energy* **2021**, *1*, 100006.
[2] Q. Hou, X. Qi, M. Zhen, H. Qian, Y. Nie, C. Bai, S. Zhang, X. Bai, M. Ju, *Green Chem.* **2021**, *23*, 119–231.
[3] a) D. M. Alonso, J. Q. Bond, J. A. Dumesic, *Green Chem.* **2010**, *12*, 1493–1513; b) O. O. James, S. Maity, L. A. Usman, K. O. Ajanaku, O. O. Ajani, T. O. Siyanbola, S. Sahu, R. Chaubey, *Energy Environ. Sci.* **2010**, *3*, 1833–1850.
[4] R.-J. van Putten, J. C. van der Waal, E. de Jong, C. B. Rasrendra, H. J. Heeres, J. G. de Vries, *Chem. Rev.* **2013**, *113*, 1499–1597.
[5] a) Y. Román-Leshkov, C. J. Barrett, Z. Y. Liu, J. A. Dumesic, *Nature* **2007**, *447*, 982–985; b) G.-H. Wang, J. Hilgert, F. H. Richter, F. Wang, H.-J. Bongard, B. Spliethoff, C. Weidenthaler, F. Schüth, *Nat. Mater.* **2014**, *13*, 293–300; c) R. Goyal, B. Sarkar, A. Bag, N. Siddiqui, D. Dumbre, N. Lucas, S. K. Bhargava, A. Bordoloi, *J. Catal.* **2016**, *340*, 248–260.
[6] G. W. Huber, J. N. Chheda, C. J. Barrett, J. A. Dumesic, *Science* **2005**, *308*, 1446–1450.
[7] D. Liu, E. Y.-X. Chen, *ChemSusChem* **2013**, *6*, 2236–2239.
[8] Y.-B. Huang, Z. Yang, J.-J. Dai, Q.-X. Guo, Y. Fu, *RSC Adv.* **2012**, *2*, 11211–11214.
[9] a) B. A. Frontana-Uribe, R. D. Little, J. G. Ibanez, A. Palma, R. Vasquez-Medrano, *Green Chem.* **2010**, *12*, 2099–2119; b) O. Simoska, Z. Rhodes, S. Weliwatte, J. R. Cabrera-Pardo, E. M. Gaffney, K. Lim, S. D. Minteer, *ChemSusChem* **2021**, *14*, 1674–1686; c) A. Wiebe, T. Gieshoff, S. Möhle, E. Rodrigo, M. Zirbes, S. R. Waldvogel, *Angew. Chem. Int. Ed.* **2018**, *57*, 5594–5619; *Angew. Chem.* **2018**, *130*, 5694–5721.
[10] a) X. H. Chadderdon, D. J. Chadderdon, T. Pfennig, B. H. Shanks, W. Li, *Green Chem.* **2019**, *21*, 6210–6219; b) H. Liu, T.-H. Lee, Y. Chen, E. W. Cochran, W. Li, *Green Chem.* **2021**, *23*, 5056–5063.
[11] a) Y. Kwon, Y. Y. Birdja, S. Raoufmoghaddam, M. T. M. Koper, *ChemSusChem* **2015**, *8*, 1745–1751; b) Y. Kwon, E. de Jong, S. Raoufmoghaddam, M. T. M. Koper, *ChemSusChem* **2013**, *6*, 1659–1667; c) L. Zhang, F. Zhang, F. C. Michel Jr., A. C. Co, *ChemElectroChem* **2019**, *6*, 4739–4749; d) J. J. Roylance, T. W. Kim, K.-S. Choi, *ACS Catal.* **2016**, *6*, 1840–1847; e) G. Sanghez de Luna, P. H. Ho, A. Lolli, F. Ospitali, S. Albonetti, G. Fornasari, P. Benito, *ChemElectroChem* **2020**, *7*, 1238–1247; f) G. Sanghez de Luna, P. H. Ho, A. Sacco, S. Hernández, J.-J. Velasco-Vélez, F. Ospitali, A. Paglianti, S. Albonetti, G. Fornasari, P. Benito, *ACS Appl. Mater. Interfaces* **2021**, *13*, 23675–23688.
[12] a) X. H. Chadderdon, D. J. Chadderdon, J. E. Matthiesen, Y. Qiu, J. M. Carraher, J.-P. Tessonnier, W. Li, *J. Am. Chem. Soc.* **2017**, *139*, 14120–14128; b) X. Shang, Y. Yang, Y. Sun, *Green Chem.* **2020**, *22*, 5395–5401; c) W. C. Albert, A. Lowy, *Trans. Electrochem. Soc.* **1939**, *75*, 367.
[13] J. Wang, H. Kong, J. Zhang, Y. Hao, Z. Shao, F. Ciucci, *Prog. Mater. Sci.* **2021**, *116*, 100717.
[14] P. Anastas, N. Eghbali, *Chem. Soc. Rev.* **2010**, *39*, 301–312.
[15] A. Dekanski, J. Stevanović, R. Stevanović, B. Ž. Nikolić, V. M. Jovanović, *Carbon* **2001**, *39*, 1195–1205.
[16] Y. Einaga, J. S. Foord, G. M. Swain, *MRS Bull.* **2014**, *39*, 525–532.

[17] G. R. Salazar-Banda, A. E. de Carvalho, L. S. Andrade, R. C. Rocha-Filho, L. A. Avaca, *J. Appl. Electrochem.* **2010**, *40*, 1817–1827.
[18] J. Xu, M. C. Granger, Q. Chen, J. Strojek, T. Lister, G. Swain, *Anal. Chem.* **1997**, *69*, 591 A-597 A.
[19] P. Nilges, U. Schröder, *Energy Environ. Sci.* **2013**, *6*, 2925–2931.
[20] a) Y. Zhou, Y. Shen, X. Luo, *Catal. Sci. Technol.* **2021**, *11*, 4882–4888; b) D.-H. Nam, B. J. Taitt, K.-S. Choi, *ACS Catal.* **2018**, *8*, 1197–1206.
[21] R. Kloth, P. Khanipour, K. J. J. Mayrhofer, I. Katsounaros, *Rapid Commun. Mass Spectrom.* **2021**, *35*, e9091.
[22] W. Schmickler, E. Santos, in *Interfacial Electrochemistry*, Springer Berlin Heidelberg, Berlin, Heidelberg, **2010**, pp. 163–175.
[23] I. Katsounaros, J. C. Meier, S. O. Klemm, A. A. Topalov, P. U. Biedermann, M. Auinger, K. J. J. Mayrhofer, *Electrochem. Commun.* **2011**, *13*, 634–637.
[24] L. A. Hutton, J. G. Iacobini, E. Bitziou, R. B. Channon, M. E. Newton, J. V. Macpherson, *Anal. Chem.* **2013**, *85*, 7230–7240.
[25] a) P. Khanipour, M. Löffler, A. M. Reichert, F. T. Haase, K. J. J. Mayrhofer, I. Katsounaros, *Angew. Chem. Int. Ed.* **2019**, *58*, 7273–7277; *Angew. Chem.* **2019**, *131*, 7351–7355; b) A. K. Schuppert, A. A. Topalov, I. Katsounaros, S. O. Klemm, K. J. J. Mayrhofer, *J. Electrochem. Soc.* **2012**, *159*, F670–F675.
[26] N. Martić, C. Reller, C. Macauley, M. Löffler, A. M. Reichert, T. Reichbauer, K.-M. Vetter, B. Schmid, D. McLaughlin, P. Leidinger, D. Reinisch, C. Vogl, K. J. J. Mayrhofer, I. Katsounaros, G. Schmid, *Energy Environ. Sci.* **2020**, *13*, 2993–3006.
[27] D. van der Vliet, D. S. Strmcnik, C. Wang, V. R. Stamenkovic, N. M. Markovic, M. T. M. Koper, *J. Electroanal. Chem.* **2010**, *647*, 29–34.

Manuscript received: July 26, 2021
Revised manuscript received: September 21, 2021
Accepted manuscript online: September 22, 2021
Version of record online: October 25, 2021